Published online 9 November 2012 *Nucleic Acids Research, 2013, Vol. 41, No. 1* ***167–181***
doi:10.1093/nar/gks1031

Single-molecule kinetics reveal microscopic mechanism by which High-Mobility Group B proteins alter DNA flexibility

Micah J. McCauley[1], Emily M. Rueter[2], Ioulia Rouzina[3], L. James Maher III[2] and Mark C. Williams[1,*]

[1]Department of Physics, Northeastern University, Boston, MA 02115, [2]Department of Biochemistry and Molecular Biology, Mayo Clinic College of Medicine, Rochester, MN 55905 and [3]Department of Biochemistry, Molecular Biology and Biophysics, University of Minnesota, Minneapolis, MN 55455, USA

Received August 14, 2012; Revised October 2, 2012; Accepted October 5, 2012

ABSTRACT

Eukaryotic High-Mobility Group B (HMGB) proteins alter DNA elasticity while facilitating transcription, replication and DNA repair. We developed a new single-molecule method to probe non-specific DNA interactions for two HMGB homologs: the human HMGB2 box A domain and yeast Nhp6Ap, along with chimeric mutants replacing neutral N-terminal residues of the HMGB2 protein with cationic sequences from Nhp6Ap. Surprisingly, HMGB proteins constrain DNA winding, and this torsional constraint is released over short timescales. These measurements reveal the microscopic dissociation rates of HMGB from DNA. Separate microscopic and macroscopic (or local and non-local) unbinding rates have been previously proposed, but never independently observed. Microscopic dissociation rates for the chimeric mutants ($\sim$10 s^{-1}) are higher than those observed for wild-type proteins ($\sim$0.1–1.0 s^{-1}), reflecting their reduced ability to bend DNA through short-range interactions, despite their increased DNA-binding affinity. Therefore, transient local HMGB–DNA contacts dominate the DNA-bending mechanism used by these important architectural proteins to increase DNA flexibility.

INTRODUCTION

High-mobility group (HMG) proteins are abundant nuclear proteins that support a range of cellular functions, from nuclear re-organization and DNA repair to cellular signaling (1–4). Within the hierarchy of HMG proteins and binding motifs, the HMGB subgroup is characterized by non–sequence-specific DNA binding. In eukaryotes, roughly 1 HMGB protein exists for every 10 nucleosomes (5). While histones organize DNA into chromatin, HMGB proteins induce bending of bare DNA, increase apparent DNA flexibility and have been proposed to weaken nucleosome structure, a necessary prelude to transcription (1,6,7). Specifically, while linker histone H1 inhibits nucleosome sliding and promotes chromatin condensation, HMGB proteins may dislocate DNA–histone contacts, although it is unknown whether binding is preferentially to the linker sequence or directly to the nucleosome (8,9). HMGB proteins bind to the DNA minor groove strongly, unwinding and bending the DNA and enhancing the local flexibility of the double helix. HMGB proteins may influence transcriptional regulation by enhancing DNA flexibility, stabilizing looping and serving as chaperones for transcription factors (10–12).

HMGB proteins carry one or two copies of a highly conserved 'HMG box' motif of $\sim$80 amino acids, together with charged N- or C-terminal tail domains (13). As shown in Figure 1 [box A of human HMGB2 and the single-box protein Nhp6Ap, an HMGB1 homologue found in *Saccharomyces cerevisiae* (14–17)], a single HMG box comprises three α helices. The L-shaped structure is partially stabilized by hydrophobic contacts between the α helices, although the final structure is stable only on binding to DNA. These proteins bind into the minor groove of DNA with little sequence specificity (10). At the binding interface lie a primary intercalating residue and a more weakly intercalating secondary residue that perturb base pair stacking in the minor groove (Figure 1). These intercalating residues also endow HMGB proteins with a noted binding preference for bent DNA, including DNA kinked by cisplatin cross-linking (11,15,18) or cruciforms (19). HMGB cationic residues on the flexible N-terminal domain (NTD) or C-terminal domain often further enhance DNA bending, suggesting a more subtle relationship between local interactions and HMGB-induced flexibility

*To whom correspondence should be addressed. Tel: +1 617 373 7323; Fax: +1 617 373 2943; Email: mark@neu.edu

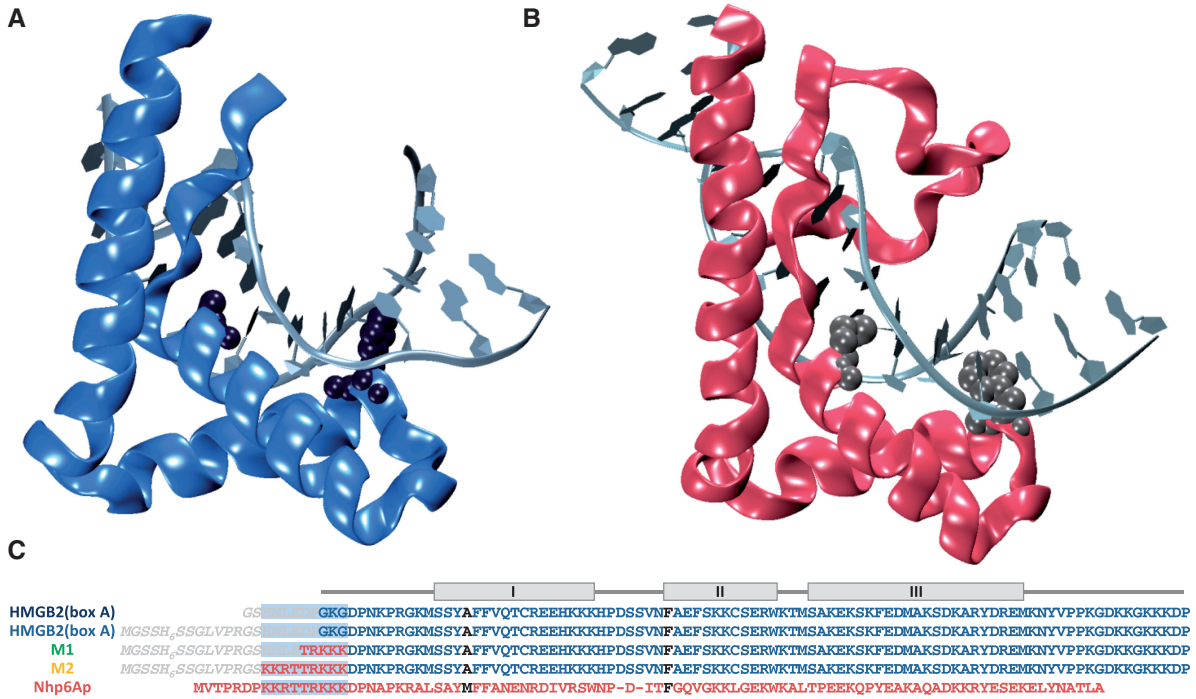

Figure 1. HMGB proteins studied in DNA–protein binding assays. (**A**) Box A of human HMGB2 bound to cisplatin-modified DNA (PDB: 1ctk) (15). Box B and the linker sequence of the tandem box structure are omitted for clarity. (**B**) Single-box domain of HMGB1 homologue Nhp6Ap from *S. cerevisiae* bound to a recognition sequence for the transcription factor SRY (PDB: 1j5n) (14). Dark spheres illustrate partial intercalators methionine in Nhp6Ap, and alanine in HMGB2 (box A), as well as the intercalating residue phenylalanine present in both. (**C**) Sequences of HMGB2 (box A), Nhp6Ap and two chimeras (termed M1 and M2) based on the box A motif (residues in blue), including cationic residues from the N-terminus of the Nhp6Ap protein (in red—the region of substituted residues is also highlighted) (5). Shaded boxes indicate helical regions, and intercalating residues are shown in black. M1 and M2 were purified with poly(His) tags as shown (in grey italics), which Nhp6Ap proteins lack. Box A of HMGB2 was studied with and without tags.

(20,21). HMGB-induced bending angles have been characterized, and estimates range from 70 to 120 degrees for various proteins (14,17,20–25). Enhanced apparent DNA flexibility may result from an ensemble of random hinges produced in DNA by transiently bound HMGB proteins (26). Atomic force microscopy analysis of the bending angles induced by HMGB2 (box A) showed a wide distribution of angles, consistent with moderately flexible transient hinges, rather than constant bending angles (27). More recent studies confirm different bend angle distributions for HMGB2 (box A) and Nhp6Ap (28). The observation of rapid association and dissociation kinetics in bulk experiments (26) seems to contradict previous observations that HMGB2 (box A) did (29) and Nhp6Ap did not (30) dissociate from DNA when the protein was removed from the solution surrounding the DNA molecule, suggesting slow dissociation kinetics.

Thus, despite significant progress in our understanding of HMGB–DNA complexes, it is crucial to clarify the kinetics of these interactions. There is some evidence that HMGB proteins polymerize on double-stranded DNA (dsDNA) at high concentrations, gradually forming filaments over long incubation times of several hours (29). Other proteins have been noted to rigidify DNA (31,32). However, it is unlikely that this mode causes DNA bending and flexibility changes, which occur at much lower protein concentrations and on shorter timescales (26,29). A recent study (30) reported slow (10^{-2} to 10^{-3} s^{-1}) DNA dissociation rates for several non–sequence-specific DNA-bending proteins (HU, Fis and Nhp6Ap) in protein-free solutions after deposition at low protein concentrations when no cooperative binding is observed. Remarkably, rates of exchange between bound and free proteins were found to be proportional to the free protein concentration (30). Kinetic regimes for HMGB/DNA interactions thus remain mysterious.

Minor groove intercalation and cationic tail positioning in the opposing major groove are known mechanisms of DNA bending by HMGB proteins (20,21,33). However, the relative importance of these two contributions to DNA bending varies between different proteins. Here we compare two distinct HMGB proteins: the yeast Nhp6A protein with strongly cationic NTD (+7 net positive charge) and strongly intercalating methionine residue versus the human HMGB2 (box A) protein, which lacks a positive NTD and has a much weaker intercalating alanine residue (Figure 1). Intact HMGB2 is a two-box protein; box A binds DNA more weakly than box B. Nhp6Ap more closely resembles the latter box. To study the effects of N-terminal cationic residues, two additional constructs were prepared that graft cationic N-terminal residues found in Nhp6Ap in place of the N-terminal amino acids of the more weakly binding HMGB2 (box A) (5). Mutant M1 adds three positive charges to the N-terminus of HMGB2 (box A), whereas M2 adds six (Figure 1C). To characterize the roles of the

N-terminal charge and intercalating residue in DNA-binding affinity, kinetics and DNA bending, these proteins were exposed to single duplex DNA molecules held and stretched within an optical tweezers apparatus (34,35). We now extend our previous studies of this system by characterizing binding affinity for relaxed and over-stretched DNA, intercalation, extent of DNA bending and exchange kinetics. These results answer key questions and provide important new insights into the molecular mechanism by which HMGB architectural proteins increase the apparent flexibility of DNA while resolving previous seemingly contradictory kinetics measurements.

MATERIALS AND METHODS

Protein expression and purification

Recombinant HMGB proteins were expressed and purified as described previously (36). Where the N-terminal hexahistidine affinity tag was removed, an immobilized thrombin reagent was used as described by the manufacturer (Thrombin CleanCleave, Sigma). Briefly, 200 µl of immobilized thrombin was used per milligram of fusion protein in 1-ml cleavage reactions incubated at 24°C for 16 h. Protein was then further purified by size exclusion chromatography in phosphate-buffered saline on a Superdex 200 10/30 column eluted at a flow rate of 0.4 ml/min. Desired fractions were pooled, dialyzed against 20 mM HEPES (pH 7.5), 100 mM KCl, 1 mM ethylenediaminetetraacetic acid and 1 mM DTT and concentrated. Proteins were stored at −20°C in this dialysis buffer supplemented with 50% (v/v) glycerol.

Optical tweezers

Phage-λ DNA, biotinylated on the opposing cohesive ends, is tethered between a pair of 5-µm-diameter streptavidin-coated polystyrene beads within an optical tweezers flow cell, as shown in Figure 2A (34,35). Experimental buffers consist of 10 mM HEPES, pH 7.5, and 100 mM Na^+. In position compliant experiments, a fast-scan piezoelectric stage moves the flow cell relative to the trap in fixed 100-nm increments. Force calibration is determined from the known overstretching transition force of DNA at specific solution and pulling rate conditions (37). Typical sets of extension and recovery data are shown in Figure 2C. Protein is introduced into solution (Figure 2B) while the tension in the DNA molecule is fixed at ~20 pN, to reduce the probability of protein-mediated loop formation (23). Cycles of extension and release are repeated in the presence of a given protein concentration. Representative cycles are shown in Figure 2D, for 400 nM of the protein Nhp6Ap.

RESULTS

Effect of HMG proteins on dsDNA elasticity

DNA force-extension curves change significantly as HMGB protein concentration is increased. Figure 2 illustrates the differences between free DNA and DNA in saturating concentrations of Nhp6Ap. Before the onset of the DNA overstretching transition at ~62 pN, the DNA and HMGB–DNA stretching curves are highly reproducible and near equilibrium at all pulling rates. Elasticity is well described by the worm-like chain (WLC) model. In this model, the polymer conformation is characterized by its contour length, B_{ds}, persistence length, P_{ds}, and optional inclusion of a phenomenological enthalpic stiffness (S_{ds}) (38,39);

$$b(F) = B_{ds}\left[1 - \frac{1}{2}\left(\frac{k_bT}{P_{ds}F}\right)^{1/2} + \frac{F}{S_{ds}}\right] \quad (1)$$

Fitting DNA force-extension data to the WLC model was first performed in the absence of protein (Figure 3A). The non-linear algorithm of Levenberg–Marquardt was used to minimize χ^2_v (40,41). Fitted values are typical and in reasonable agreement with previously published results under these solution conditions (37,38).

Figure 3A also compares the fitted protein-free DNA force-extension curve with that obtained in the presence of saturating concentrations of Nhp6Ap. Interestingly, Nhp6Ap-saturated DNA is shorter than protein-free DNA at low forces and longer than protein-free DNA at high forces (>10 pN). We interpret this effect as evidence of HMGB-induced DNA compaction by bending at low force (entropic elasticity regime), with increase of the HMGB–DNA contour length due to HMGB intercalation observed when the complex is straightened at higher forces. These effects dramatically change the fitted elastic parameters for DNA saturated by Nhp6Ap (Figure 3A). Similar results were previously obtained for DNA saturated a by single-box motif HMGB2 protein (23,29). In particular, there is a remarkable 6- to 8-fold reduction in the dsDNA persistence length, an ~10% increase in the DNA contour length and a minor change in elastic modulus on saturated binding of all HMGB proteins studied in this work. An alternative fitting scheme describes HMGB–DNA regions with the freely jointed chain model, assuming the HMGB–DNA complex is a polymer that contains a random mixture of two polymers of different elasticity: protein-free dsDNA and protein-saturated dsDNA, in Supplementary Figure S1 and Supplementary Table S1.

Interestingly, there is no evidence that these HMGB proteins dissociate from DNA owing to applied force, even up to 200 pN. Overstretching curves are reproducible even after several cycles of extension and release (Figure 2), even up to forces of 200 pN (see Figure 5). The ability of the applied force to straighten the HMG-bent DNA without protein dissociation indirectly supports one of the major conclusions of this work: HMGB-type proteins bend DNA by introducing flexible transient hinges, rather than rigid fixed DNA bends. This may reflect the ability of HMGB proteins to both compact DNA by bending and elongate DNA by intercalation. While applied force tends to dissociate proteins that shorten DNA (42), force promotes DNA binding for proteins that elongate DNA (43). Given that our data are reproducible over several cycles of stretch and release, and that changes in the measured properties

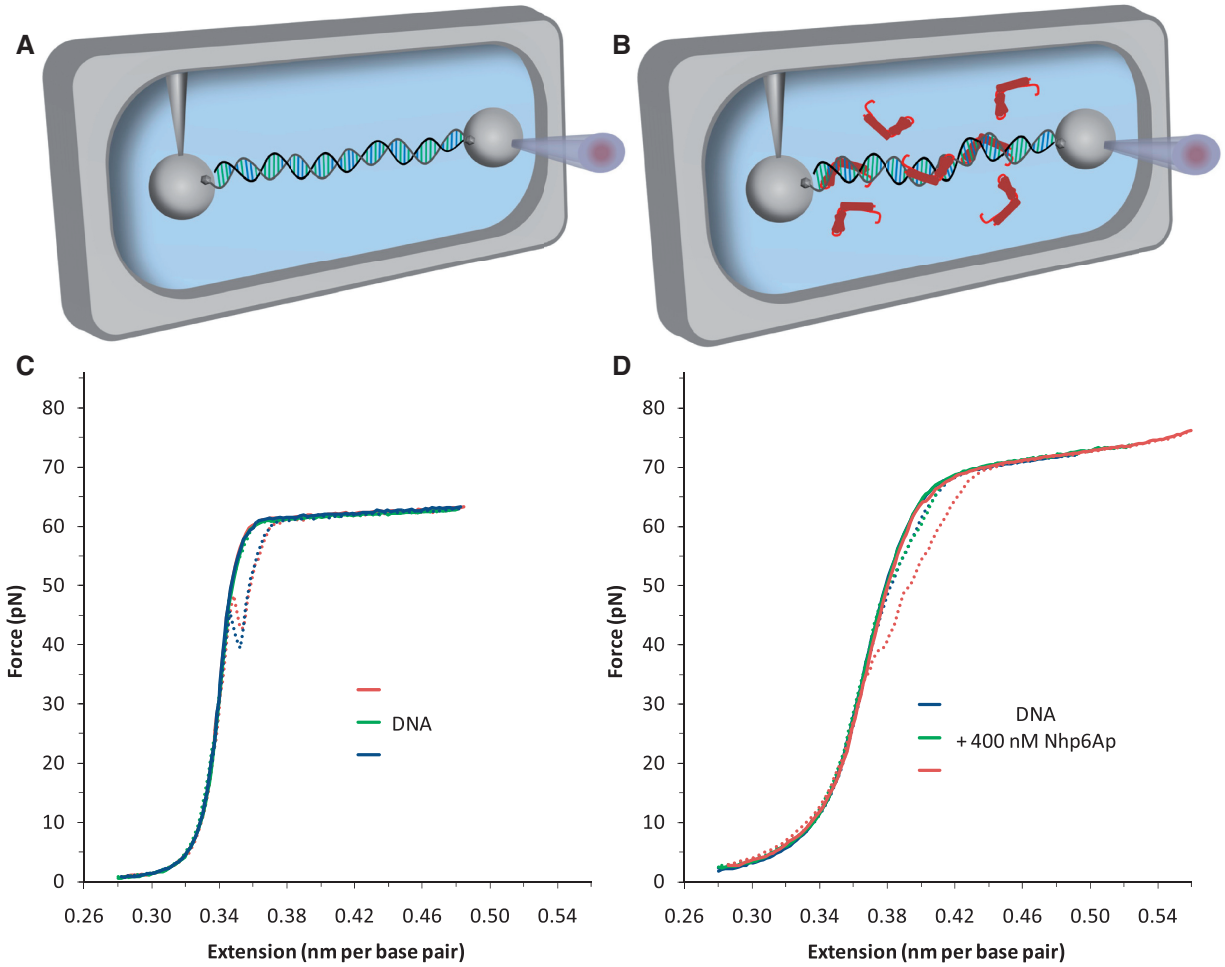

Figure 2. Cycles of extension and release for DNA in an optical tweezers experiment. (**A**) DNA is tethered within a flow cell and extended between functionalized spheres. (**B**) DNA is extended in a solution containing HMGB protein. (**C**) Phage-λ DNA (48 500 bp in length) is extended (solid line) and overstretched at ~60 pN. Release (dotted line) indicates that the process is reversible on the timescales of these experiments. Three sequential cycles of extension and recovery (shown in red, green and blue) illustrate the reproducibility of the data. (**D**) When DNA is exposed to a solution including 400 nM Nhp6Ap, three extension and release cycles (blue, green and red) reveal consistent changes in the persistence length, contour length and the overstretching force.

appear to vary smoothly with protein concentration (see below), it is reasonable to assume that the fractional HMGB saturation of DNA, Θ, is approximately independent of force and determined by the bulk protein concentration.

Figure 3B and C present the concentration dependences of the fitted persistence length, $P_{ds}(c)$, and contour length, $B_{ds}(c)$. A simple model assumes that DNA-bending events are statistically independent, and independent of DNA-bending modes observed in the absence of protein. The reciprocals of the protein-free P_D and protein-saturated P_L values may be averaged, weighting by the fractional DNA site occupancy, Θ, to yield the observed persistence length (P) (44,45):

$$P_{ds}(\Theta) = \frac{P_L \cdot P_D}{P_L + \Theta \cdot (P_D - P_L)} \quad (2)$$

Variation of DNA occupancy by protein, Θ, as a function of c is described by a binding isotherm. We applied the McGhee–von Hippel isotherm (46,47), conventionally used for the description of polymeric DNA–protein binding:

$$\Theta = \frac{cn}{K_D}(1-\Theta) \left[\frac{(2\omega-1)(1-\Theta)+\Theta/n-R}{2(\omega-1)(1-\Theta)}\right]^{n-1} \left[\frac{1-(n+1)\cdot\Theta/n+R}{2(1-\Theta)}\right]^{2} \quad (3)$$

where

$$R = \sqrt{(1-(n+1)\cdot\Theta/n)^2 + \frac{4\omega\Theta}{n}(1-\Theta)}$$

Here K_D, n and ω are the equilibrium protein–DNA dissociation constant, binding site size in base pairs and binding cooperativity parameter, respectively. The DNA-binding site size ($n = 7$) for all HMGB single-box proteins was estimated from crystal structures of protein–DNA complexes, such as HMGB (box A) presented in Figure 1, and others (48). The value of the HMGB–DNA

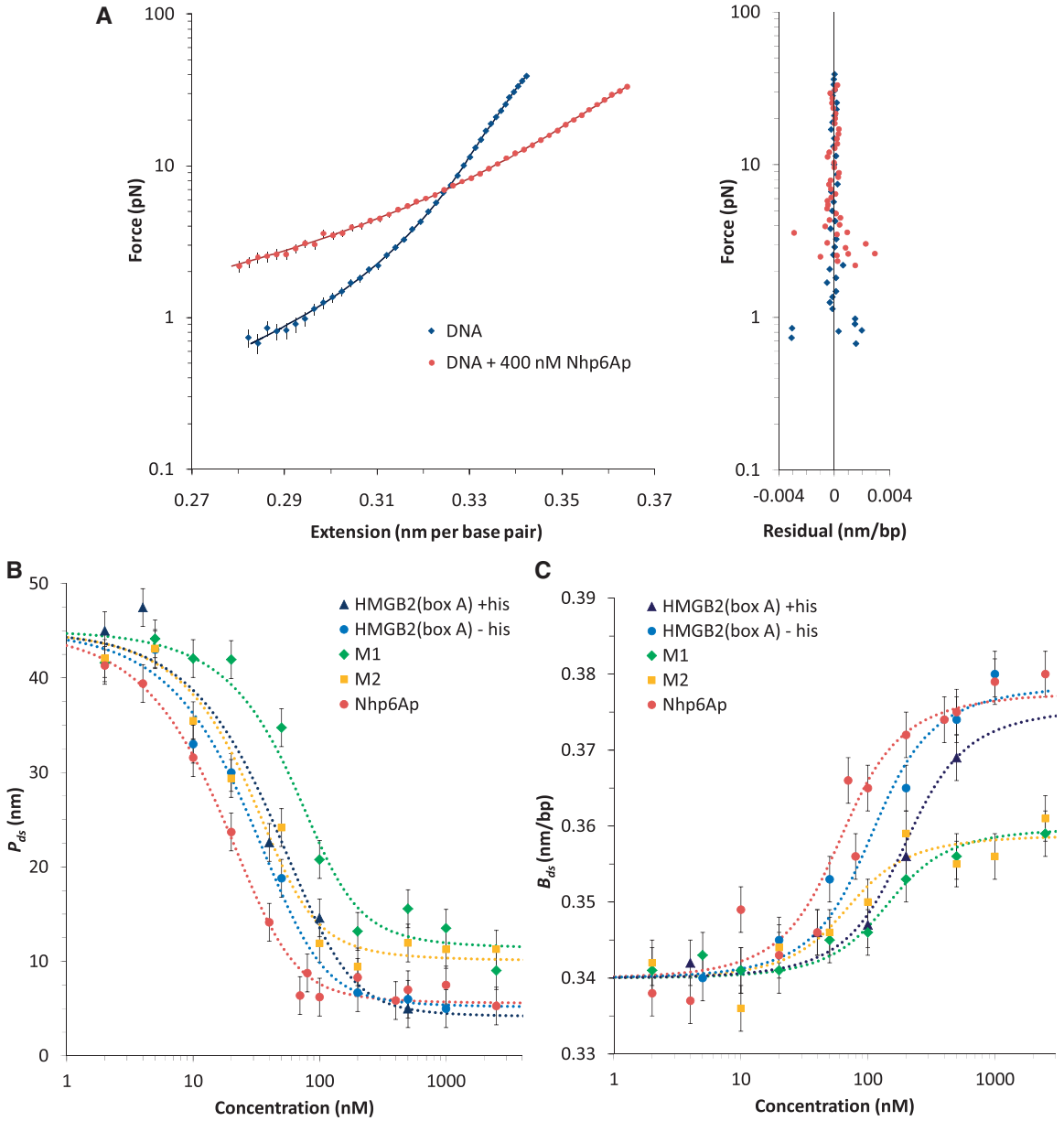

Figure 3. Quantifying DNA–protein elasticity. (**A**) The extension data (solid symbols) of a typical single extension cycle for DNA (blue diamonds) and DNA in the presence of 400 nM Nhp6Ap (red circles). Vertical bars represent standard error of measurement when larger than symbols. Fits to the WLC model for bare DNA (blue line) provided values of $P_{ds} = 48 \pm 2$ nm, $B_{ds} = 0.340 \pm 0.002$ nm/bp and $S_{ds} = 1400 \pm 100$ pN ($\chi^2_v = 0.45$). When the DNA was exposed to 400 nM Nhp6Ap (red line), these fitted values became $P_{ds} = 6.7 \pm 0.7$ nm, $B_{ds} = 0.380 \pm 0.002$ nm/bp and $S_{ds} = 1240 \pm 200$ pN ($\chi^2_v = 0.37$). Residuals to these fits are shown on the right. (**B**) Fitted HMGB–DNA persistence length, $P_{ds}(c)$, determined versus concentration of Nhp6Ap (red), constructs M1 (green) and M2 (yellow) and HMGB2 (box A) proteins with and without an N-terminal poly(His) tag (blue and cyan). Symbols represent averages of fitted parameters from three to six fitted data sets. Lines indicate fits to Equations 2 and 3, to determine the equilibrium constant, K_D, and the persistence length of DNA saturated with protein, P_L. (**C**) The HMGB–DNA contour length, $B_{ds}(c)$, fit to Equations 2 and 4, to determine the contour length of DNA saturated with protein, B_L. The value of K_D is indistinct from the fits of Figure 3B. All fits assume a fixed binding site size ($n = 7$) and weak cooperativity ($\omega = 20$), while χ^2_v ranges from 0.5 to 2.0. Fitted parameters for all proteins are summarized in Table 1.

binding cooperativity parameter that best fits P_{ds}(c) and B_{ds}(c) dependencies was found to be $\omega = 20$ for all fits, corresponding to a free energy of protein–protein interaction, $k_B T \cdot \ln \omega$, of 1.7 kcal/mol. This indicates weak cooperativity of HMGB binding, as previously observed (27,49). The persistence length of bare DNA (P_D) was fixed at 45 nm, such that the only free fitting parameters were P_L and K_D. Best-fit values of these parameters are then summarized in Table 1. An alternative fitting procedure using the Hill binding isotherm, presented in Supplementary Figure S2 and Table S2, yields Hill parameters ranging from 1 to 1.5, also consistent with weakly cooperative HMGB–DNA binding. Variations in any results due to the presence of the his_6 tags were minor, and these differences are considered explicitly in Supplementary Tables S3 and S4.

The DNA contour length increases by up to 10% in the presence of HMGB proteins, confirming the intercalative

nature of HMGB–DNA binding. While this is a relatively small effect compared with the major reduction of persistence length by HMGB proteins, it implies DNA elongation by the equivalent of a single base pair (0.34 nm) for every 10 bp. Taking into account that each HMGB protein binds to at least 7 bp and has a single primary intercalating aromatic residue, our result suggests an almost complete intercalation of this residue, comparable with the DNA elongation on intercalation of conventional intercalators, such as ethidium and intercalating ruthenium complexes (43). Quantitatively, the DNA contour length increases owing to independent HMGB-binding events that add to the overall length, in proportion to their occupancy (Θ):

$$B_{ds}(\gamma) = B_D + \Theta \cdot (B_L - B_D) \quad (4)$$

As above, the binding site size is fixed at $n = 7$ bp, $\omega = 20$ and $B_D = 0.34$ nm/bp. This leaves only K_D and B_L as free parameters for the fits to Equations 2 and 4, which are shown in Figure 3C, and collected in Table 1.

Using models of polymer elasticity, the decrease in the apparent DNA persistence length due to the protein binding can be further related to the average DNA-bending angle, β, associated with individual protein-binding events. Assuming independent binding/bending events and taking into account that one protein binds per $n \cdot B_L$ length of dsDNA at saturation, β can be related to the measured saturated persistence length P_L (44,45,50,51):

$$\langle \beta \rangle = \cos^{-1}\left(\frac{2P_L - nB_L}{2P_L + nB_L}\right) \quad (5)$$

Calculated β values are summarized in Table 1.

The fact that K_d values obtained by fitting two independently measured characteristics of the HMGB–DNA complex, $P_{ds}(c)$ and $B_{ds}(c)$, are in excellent agreement confirms our ability to characterize protein binding under applied force. Fitted binding affinities for all four HMGB proteins summarized in Table 1 correlate with the positive charge of the NTD as previously suggested (5). In contrast, saturated values of the HMGB–DNA complex persistence length P_L, contour length B_L and bending angle per protein β do not correlate with NTD positive charge (Table 1). Similar 10-fold reductions in DNA persistence length are induced by the two wild-type proteins, HMGB2 (box A) and Nhp6A, despite different NTD charges. The effects of the two chimeric HMGB proteins with altered NTD residues are approximately a factor of two weaker.

We previously observed the formation of a rigid HMGB–DNA filament at much higher HMGB concentrations (>10 μM) and on longer timescales of several hours (29). Filament formation has also been observed for HU, a functional analog of HMGB found in bacteria (31,52). However, HU-induced dsDNA bending and compaction were directly followed by dsDNA straightening as HU concentration was increased. Filament formation at HU concentrations leading to DNA straightening resulted in slower HU dissociation kinetics (52). In contrast, as shown in this work, increasing HMGB concentration well below 10 μM leads to saturated protein binding and a 10-fold reduction in DNA persistence length without filament formation. Thus, HMGB effects on DNA discussed here are not directly related to HMGB–HMGB interactions inducing filament formation at much higher HMGB concentrations.

Effect of HMGB proteins on equilibrium DNA strand pairing stability

Thus far, we have considered HMGB effects on DNA elasticity before the onset of the force-induced overstretching transition in dsDNA. During this transition, the two DNA strands are unwound and stretched to almost twice their B-form length. The nature of the overstretching transition is still under investigation (53–58), but the observed increase in overstretching force required in the presence of protein binding indicates preferential HMGB stabilization of B-form dsDNA (Figure 4A). The DNA overstretching transition appears to be reversible in the presence of HMGB protein, such that DNA stretching and release curves overlap, and are independent of the pulling rate when the DNA is stretched at the rate of 100 nm/s or slower. Because the total λ-DNA extension increases by ~10 μm during overstretching, equilibrium is preserved on the timescale of ~100 s or longer. We now analyze HMGB protein effects in this overstretching regime to gain important new insights.

For this purpose, we define the overstretching force, F_{ov}, as a transition midpoint force averaged between DNA extension per base pair values of 0.42 and 0.48 nm. In the absence of proteins, F_{ov} is known to vary with solution ionic strength, pH and temperature (37,59,60). Under our experimental conditions (100 mM Na^+, 21°C, pH 7.5), $F_{ov} = 62.6 \pm 0.4$ pN, in accord with previous studies. Figure 4A shows that a saturating Nhp6Ap concentration increases F_{ov} to ~73 pN. This increase in the transition force characterizes the equilibrium preferential binding of HMGB protein (per base pair) to B-form DNA, relative to the overstretched state: $\delta G = \delta F \cdot \Delta x \approx 0.5\, k_B T$. For a binding site size of $n = 7$, this implies preferential HMGB protein binding to B-form DNA that is a factor of $e^{n\Delta x \cdot \delta F / k_b T} \approx e^3 \approx 20$ stronger than to overstretched DNA. This factor of 20 preference for B-form DNA (which is similar to the measured cooperativity parameter ω) may simply reflect the loss of cooperative HMGB–HMGB binding interactions on overstretching without the release of HMGB–DNA contacts. Complete DNA overstretching is typically observed in the presence of bound protein which argues against filament formation (Figure 2D). The high reproducibility of DNA stretch–release curves even under saturating protein concentrations suggests that HMGB proteins remain bound throughout the stretching cycle, accommodating the transition from B-form DNA to overstretched DNA on a timescale longer than 100 s. Additional support for this hypothesis comes from the fact that faster DNA overstretching reveals non-equilibrium protein effects on the overstretching transition, as discussed below. It is exactly this insight that

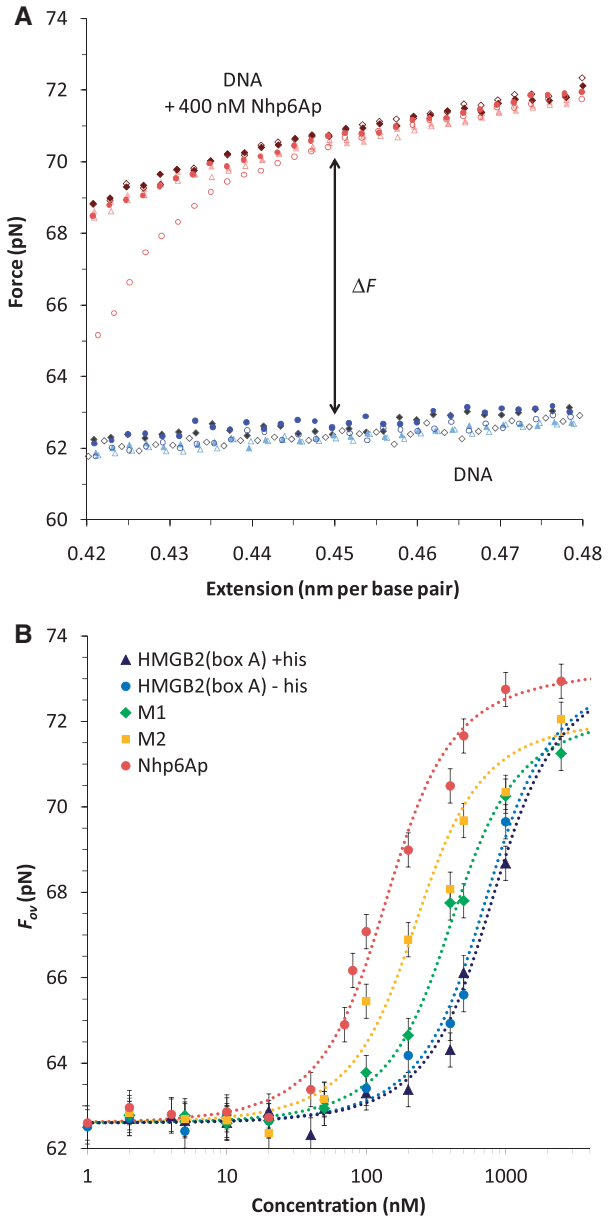

Figure 4. Quantifying DNA–protein stability. (**A**) The overstretching force for a DNA molecule (blue circles, triangles and diamonds) rises when that molecule is exposed to 400 nM Nhp6Ap (red circles, triangles and diamonds). The extension data of three contiguous cycles of extension (solid symbols) and release (open symbols) are plotted to illustrate the reproducibility of the data. Averaging extensions over the range of the graph (0.42–0.48 nm per base pair), and over each of the three cycles, the overstretching force is found to be 62.4 ± 0.4 pN in the absence and 70.2 ± 0.4 pN in the presence of 400 nM Nhp6Ap. (**B**) The observed overstretching force $F_{ov}(c)$ fit to the site exclusion binding isotherm of Equations 3 and 6 to determine K_D and the overstretching force of DNA saturated with protein, F_{ov}^L. All fits assume a fixed binding site size (n = 7) and weak cooperativity (ω = 20), while χ_v^2 ranges from 0.5 to 2.0. Fitted parameters are found in Table 2.

permits estimation of DNA dissociation times for individual HMGB proteins.

Assuming that $F_{ov}(c)$ increases linearly with the amount of HMGB protein bound to DNA, the complete $F_{ov}(c)$ dependence presented in Figure 4B can be fit to the binding isotherm given by Equation (2) using the expression

$$F_{ov}(\Theta) = F_{ov}^D + \Theta \cdot \left(F_{ov}^L - F_{ov}^D\right) \quad (6)$$

Here F_{ov}^D and F_{ov}^L are the protein-free and protein-saturated values of F_{ov}. We fit the experimental $F_{ov}(c)$ to Equation 6, with $\Theta(c)$ given by the McGhee–von Hippel isotherm (Equation 3). Fits appear in Figure 4B, and the resulting equilibrium dissociation constants (K_D) and saturated melting forces (F_{ov}^L) are shown in Table 2. Interestingly, the K_D values obtained from $F_{ov}(c)$ fits are ~4-fold higher than the K_D values obtained by fitting the $P_{ds}(c)$ and $B_{ds}(c)$ dependencies (compare K_D values in Table 1 and 2). There are many possible reasons for this minor discrepancy, such as an inaccurate description of the protein effect on the transition force by the empirical relationship given in Equation 6. Fits of $F_{ov}(c)$ to the Hill isotherm are shown in Supplementary Figure S3 and Table S5. Most importantly, consistent K_D variations between the four HMGB proteins studied in this work suggest that in all cases, we are measuring the characteristics of the same binding process. K_D decreases (reflecting stronger binding affinity) with increasing charge on the NTD of the HMGB protein, in accord with the previous bulk solution measurements (5).

HMGB proteins torsionally constrain B-form DNA, inhibiting unwinding and re-winding on short timescales

As discussed above, equilibrium values of $F_{ov}(c)$ in the presence of HMGB proteins can only be observed if the DNA stretching time is ≥100 s, i.e. when the DNA is pulled at the rates slower than 100 nm/s. However, it is possible to probe DNA–ligand interactions on much shorter timescales by measuring forces at much faster DNA extension rates. This is accomplished by decreasing the signal averaging of the detector, allowing pulling rates to increase up to 50 000 nm/s, thereby reducing the total DNA stretching time to ~0.2 s. In the presence of HMGB proteins, cycles of extension and recovery at increasing pulling rates show increased overstretching forces relative to bare DNA. Figure 5A and B show responses for HMGB2 (box A) and the mutant M1 at near-saturating concentrations of protein ($c \geq K_D$). Additional data are shown in Supplementary Figure S4. As the rate of extension increases, the DNA transition force grows steeply from the protein-saturated equilibrium value $F_{ov}^L \sim 73$ pN to $F_{ov}^T \sim 115$ pN, far more than the transition force for bare DNA (Figure 5C). In the absence of protein, there is a weak dependence of the overstretching force on the pulling rate, and DNA remains close to equilibrium during overstretching (61). In the presence of HMGB, the transition force changes over a relatively narrow range of pulling rates around some characteristic rate, v_{HMG}, which is unique for each protein. The maximum transition force, $F_{ov}^T \sim 115$ pN, is the same for the four HMGB proteins studied in this work and is similar to the overstretching force observed for bare but torsionally constrained DNA (55,62).

While the stretching transition force (~115 pN) is well defined for sufficiently high protein concentration

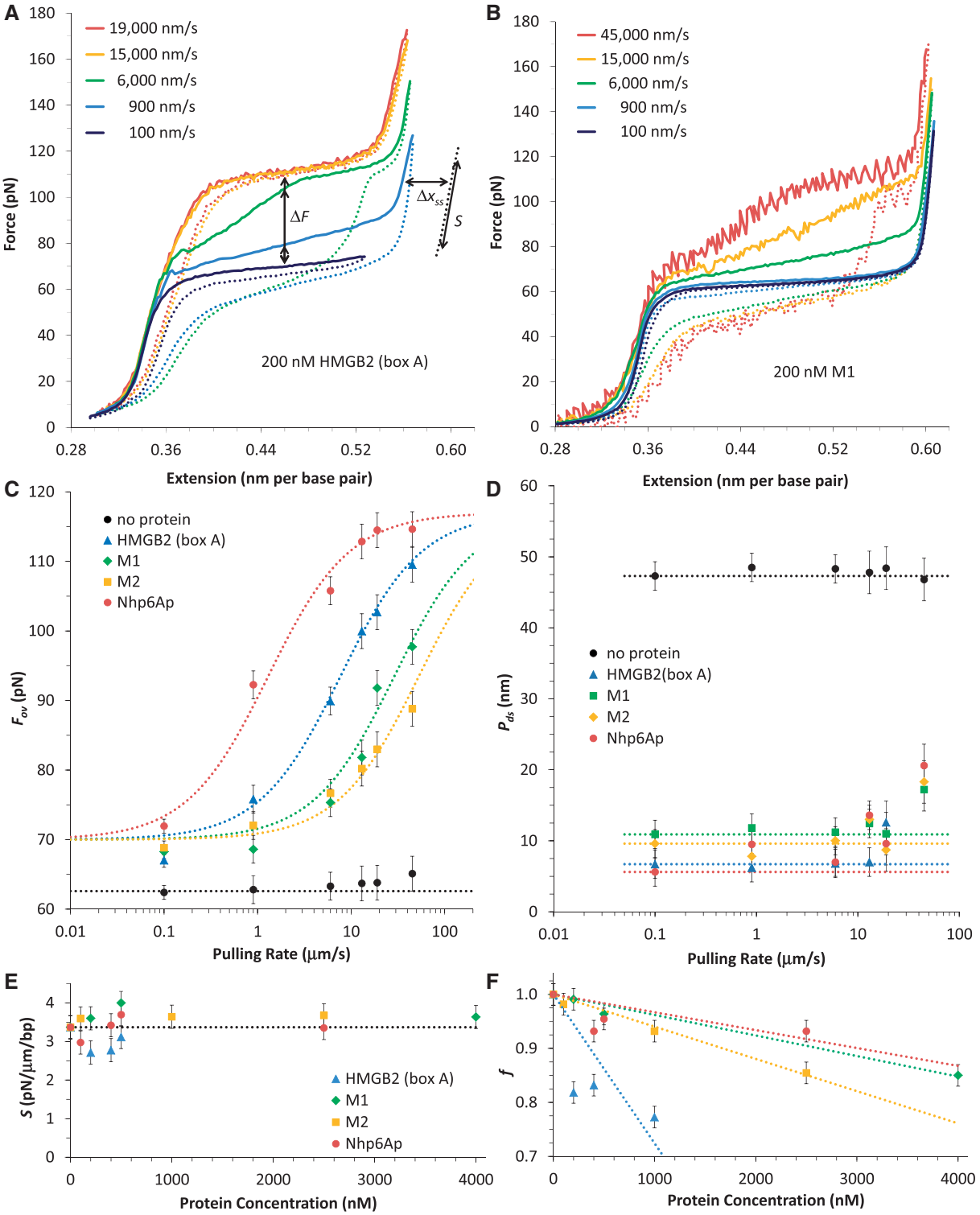

Figure 5. Probing the dynamics of HMGB–DNA binding. (**A**) Cycles of extension and release (solid and dotted lines) for (A) 200 nM HMGB2 (box A) and (**B**) 200 nM M1 as a function of the rates shown (additional data can be found in Supplementary Figure S4). At pulling rates higher than the natural dissociation rate, DNA becomes torsionally constrained. Release to lower DNA extensions shows multiple plateaus, described in the text. (**C**) The average overstretching force as a function of the experimental pulling rate, v, for bare DNA (black) and DNA exposed to Nhp6Ap (red), constructs M1 (green) and M2 (yellow) and HMGB2 (box A) (blue) proteins. Data are averaged over active concentrations ($c > K_D$) as described in the text (and Supplementary Figure S5). Dotted lines are fits to Equation 8, giving the dissociation rate, k_{off}. Rates from these fits are shown in Table 2. (**D**) Fits to Equation 1 measure P_{ds} for bare DNA (black), 500 nM Nhp6Ap (red), 2500 nM M2 (yellow), 4000 nM M1 (green) and 200 nM HMGB2. Dotted lines mark values at the lowest pulling rate (100 nm/s). (**E**) The measured stiffness, S, of the HMGB–DNA complexes after overstretching, at low pulling rates (<1000 nm/s). (**F**) The fraction of DNA that is melted by force, f, decreases with increasing protein concentration, as dsDNA is progressively converted into a stable filament that cannot be overstretched at the observed forces.

Table 1. Comparisons of the flexibility of DNA in the presence of HMG single-box binding proteins, arranged by net charge of the N-terminus (q_N) (the substituted residues of Figure 1C)

Protein	q_N	P_L(nm)	B_L(nm/bp)	S_L(pN)	K_D(nM)	β(°)
HMGB2 (box A)[a]	−1	4.6 ± 0.5	0.378 ± 0.001	1600 ± 200	180 ± 30	57 ± 4
M1	3	11.3 ± 1.1	0.360 ± 0.002	1600 ± 200	170 ± 30	37 ± 4
M2	7	10.0 ± 1.0	0.359 ± 0.002	1200 ± 200	81 ± 16	39 ± 4
Nhp6Ap	7	5.5 ± 0.5	0.378 ± 0.002	1000 ± 200	71 ± 14	52 ± 5

The values of the persistence length, contour length and stiffness of DNA in saturating concentrations of ligand are shown as P_L, B_L and S_L, respectively. These parameters and the equilibrium dissociation constant (K_D) were determined by fitting the concentration dependence of the persistence length, P_{ds}(c), and contour length, $B_{ds}(c)$, to Equations 2, 3 and 4, with fits shown in Figure 3B and C (the results for K_D are the same within uncertainty). The binding site size was assumed constant for all proteins at $n = 7$, and the cooperativity was also fixed at $\omega = 20$. Mean bending angles (β) were calculated from Equation 5.
[a]K_D and β are values averaged for HMGB samples prepared with and without poly(His) tags, which showed only minor differences. Values for proteins with and without the tags are shown distinctly in Supplementary Table S3.

Table 2. Comparisons of the stability and kinetics of HMGB–DNA interactions, arranged by net charge of the N-terminus (q_N)

Protein	q_N	F^L_{ov}(pN)	K_D(nM)	k_{off}(s^{-1})	k_a($\times 10^8 M^{-1}\ s^{-1}$)
HMGB2 (box A)[a]	−1	73.3 ± 0.2	880 ± 70	0.88 ± 0.09	0.010 ± 0.002
M1	3	72.3 ± 0.3	480 ± 60	3.3 ± 0.5	0.069 ± 0.017
M2	7	72.2 ± 0.3	260 ± 30	6.1 ± 0.7	0.23 ± 0.05
Nhp6Ap	7	73.3 ± 0.3	160 ± 20	0.15 ± 0.01	0.009 ± 0.002

Equilibrium dissociation constants (K_D) and HMGB saturated overstretching forces (F^L_{ov}) are determined from the change in $F_{ov}(c)$, fitted to Equation 3 and Equation 6 as illustrated in Figure 4B. Rate dependence experiments resolved HMGB–DNA unbinding rates (k_{off}) using fits to Equation 8, shown in Figure 5C. Unbinding rates and association rates ($k_a = k_{off}/K_D$) are deduced for each protein.
[a]K_D values averaged for HMGB prepared and without poly(His) tags. Values for proteins with and without the tags are shown distinctly in Supplementary Table S4.

($c \geq K_D$), DNA release curves vary. Sometimes the DNA release force plateau coincides with the stretching plateau at 115 pN. In other cases, however, the strand re-annealing transition occurs at a much lower (but well-defined) force of ~50 pN that is independent of the HMGB protein type (Figure 5A and B, see also Supplementary Figure S4). Furthermore, some DNA release curves begin with the strand re-annealing plateau at the higher 115 pN force, but then jump to the lower force of 50 pN. These double-plateau DNA stretching and release curves were previously observed during the stretching of torsionally constrained bare dsDNA where the degree of unwinding was fixed by immobilizing both DNA strands at both termini. DNA unwinding was then achieved by rotating the end-fixed dsDNA around its axis by a known number of turns before stretching in a magnetic tweezers apparatus (62). Relative lengths of the low and high force plateaus were determined from fractional DNA unwinding, with the transition for torsionally constrained B-form DNA at 115 pN and the transition for totally unwound dsDNA overstretching at 50 pN. Non-equilibrium DNA under-winding often persists until complete DNA release, leading to significant hysteresis in the DNA stretch-release cycle up to small forces below 50 pN. Based on HMGB-saturated dsDNA force-extension curves, we hypothesize that HMGB proteins inhibit DNA unwinding and re-winding at high pulling rates. When $v >> v_{HMG}$, both the extension and relaxation curves plateau at 115 pN with the DNA fully constrained. At rates near the characteristic rate of the protein, $v \sim v_{HMG}$, some slipping and release of strand winding occurs after complete DNA overstretching and on the onset of DNA release. This leads to the observed double plateau in the DNA release portion of the cycle, during which the DNA is trapped in a partially underwound state. In other cases, when such winding relaxation at maximum DNA extension is complete, the single DNA release plateau at ~50 pN is observed. In cases of incomplete DNA saturation with HMGB protein (at $c < K_D$), decreasing the pulling rate below v_{HMG} leads to a decrease in the force of the extension plateau, whereas the force of the release plateau rises, with both forces finally converging at the equilibrium value of ~73 pN at low pulling rates, $v << v_{HMGB}$. This observation suggests a partial HMGB protein-induced constraint on DNA unwinding and re-winding by protein concentrations below saturation. On stretching such partially torsionally constrained DNA, some unwinding may occur. However, this rate is lower than the rate of DNA unwinding imposed by overstretching, leading to increased transition force with pulling rate. These considerations suggest that on short DNA pulling timescales (0.2–10 s), HMGB proteins do not interfere with the DNA overstretching transition, but create a block to unwinding and re-winding of DNA as it is overstretched.

Importantly, the pulling rate dependence of the DNA overstretching force is only observed at higher protein concentrations ($c \geq K_D$) where the behavior of $F_{ov}(v)$ becomes highly reproducible and independent of the history of the particular DNA molecule. This observation rules out enhanced protein binding or un-binding at high forces. The effects of protein concentration are illustrated further in Supplementary Figure S5. DNA winding is apparently restricted by individual proteins bound to

both B- and overstretched forms of DNA. Complete torsional constraint would require at least one protein per helical turn of dsDNA (1 protein per 10 bp). Taking into account that each single-box HMGB-type protein covers 7 bp, this requirement amounts to fractional DNA binding of $\Theta \geq 0.7$, leading to the requirement of near-complete DNA saturation. It is important to note that complete DNA coverage by HMGB is not required for observation of the HMGB-induced DNA torsional constraint. In fact, the protein filament formation on DNA would necessarily interfere with DNA overstretching, leading to the altered length of overstretched DNA and/or irreproducible overstretching behavior resulting from random filament breaking pattern, as discussed below. If the binding of individual HMGB proteins indeed restricts DNA strand winding, the time for winding relaxation will become limited by the unbinding time of such proteins. In the context of an optical tweezers experiment, this is the time required to overstretch DNA at a given pulling rate, $v_{HMG} = N\Delta x/t$. The change in length per base pair on overstretching in the presence of HMGB is $\Delta x = x_{ds} - x_{ss} = 0.18$ nm/bp, while the total number of λ-DNA base pairs is $N = 48\,500$. An observable effect on DNA winding is anticipated when the protein dissociation time becomes similar to the DNA unwinding (overstretching) time. The desired protein dissociation rate of interest (k_{off}) can be thus found from the characteristic unwinding rate:

$$k_{off} = v_{HMGB}/N\Delta x \quad (7)$$

Fitting the experimental F_{ov} (v) dependencies for each protein presented in Figure 5C to a simple sigmoidal function determines the midpoint rate, v_{HMGB}:

$$F_{ov}(v) = F_{ov}^{L} + \frac{v}{v + v_{HMGB}}\left(F_{ov}^{T} - F_{ov}^{L}\right) \quad (8)$$

Here $F_{ov}^{L} = 73$ pN, and $F_{ov}^{T} = 115$ pN. Combining the dissociation rate k_{off} (calculated according to Equation 7 using the fitted values of v_{HMGB}) with the equilibrium dissociation constants (K_D) determined from the $F_{ov}(c)$ fit to Equation (6) allows us to estimate the association rate ($k_a = k_{off}/K_D$). These values are summarized in Table 2. Calculated k_{off} values for all four HMGB proteins studied are relatively fast, ranging between 0.1 and 10 s^{-1}, where the two wild-type HMGB proteins are the slowest [0.88 ± 0.09 and $0.15 \pm 0.01\,s^{-1}$ for HMGB2 (Box A) and Nhp6Ap, respectively], and the two chimeric HMGB proteins M1 and M2 are faster (3.3 ± 0.5 and $6.1 \pm 0.7\,s^{-1}$, respectively). Although these rates are fast, they are much slower than the unperturbed rate of protein-free DNA unwinding from free ends [$\sim 10^6\,s^{-1}$ (63)] or DNA unwinding rates limited by the rotational friction of λ-DNA (61). We conclude that it *is the actual dissociation kinetics of individual HMGB–DNA molecules that limit the DNA unwinding rate*, and use this new insight to resolve an apparent contradiction with previously measured HMGB and Nhp6Ap kinetics (29,30).

Our observation of rapid HMGB dissociation rates (complex lifetimes of 0.1–10 s) is in apparent contradiction with the much longer times (~1000 s) required to elute HMGB proteins from DNA by washing (42). We hypothesize that the fast dissociation rates measured in our DNA overstretching assays correspond to the microscopic dissociation rate, $k_{off,micro} \sim 0.1$–$10\,s^{-1}$ (42), in contrast to the macroscopic HMGB protein dissociation rate (42,64). Macroscopic dissociation describes the departure of protein from DNA into bulk solution. In contrast, microscopic dissociation involves the breaking of only short-range protein–DNA contacts, with the protein remaining within the ~1-nm range of strong electrostatic attraction (65). The latter process facilitates re-association of the same protein with DNA, while also allowing for protein exchange with other molecules in the bulk solution. We reason that microscopic HMGB–DNA dissociation events are sufficient to release the HMGB-induced torsional constraint on dsDNA unwinding and re-winding.

The double-box HMGB2 (box A + B) also exhibits rapid DNA association–dissociation kinetics

Interestingly, the double-box HMGB2 (box A + B) studied extensively in our previous work caused a comparable increase in the DNA overstretching force with increasing pulling rates, although it was not analyzed at the time (23). We have now analyzed these previous data as described above, and summarize the results in Supplementary Figure S6 and Table S6. Importantly, the double-box protein HMGB2 (box A + B) displays a dissociation rate similar to the wild-type HMGB2 (box A) and Nhp6Ap proteins. The association rate of HMGB2 (box A + B) is $\sim 10^7\,M^{-1}{\cdot}s^{-1}$, much faster than the association rate of HMGB2 (box A), leading to an ~100-fold stronger binding affinity for the HMGB2 (box A + B) compared with HMGB2 (box A) and Nhp6Ap proteins. We conclude that the double-box HMGB proteins exhibit rapid dissociation kinetics, similar to that of the single-box HMGB proteins, with two boxes contributing to net ~100-fold stronger binding and the analogous faster association rate.

DNA appears stiffer at higher pulling rates

As the melting force in the presence of HMGB grows with the pulling rate, so does the apparent DNA persistence length. Analysis of Figure 5A and B rapid stretching data (before the overstretching transition) was performed by collecting several (typically 3) extension curves and averaging. The resulting values of $P_{ds}(v)$ are shown for bare DNA and for saturating concentrations of HMGB2 (box A), M1, M2 and Nhp6Ap (Figure 5D).The persistence length shows no variation with the pulling rate for bare DNA. In the presence of HMGB protein at fast pulling rates ($v = 50\,000$ nM/s), the fitted persistence lengths increase. The maximum increase in P_L compared with its equilibrium minimal value reaches no more than 30% even at the highest pulling rates. Apparent stiffening of HMGB-bound DNA on short timescales (<1 s) could result from unwinding inhibition imposed by bound HMGB on DNA or possibly insufficient time for DNA bending by the HMGB protein.

HMGB remains bound to overstretched DNA strands without affecting their stretching behavior

After overstretching of HMGB-bound DNA, force increases steeply with extension, just as in the absence of the protein. The slope of this curve (S; see labels in Figure 5A) provides a measure of the stiffness of the overstretched HMGB–DNA complex. The stiffness is graphed for several HMGB protein concentrations in Figure 5E and compared with the value of S for bare DNA. For these protein concentrations and pulling rates, there is no measurable protein effect on the elasticity of overstretched DNA. This result is unexpected because HMGB proteins remain bound to two overstretched DNA strands as indicated by interference with strand unwinding and re-winding on timescales shorter than the dissociation time of the protein. Thus, HMGB binding to overstretched DNA strands must be compliant, as binding persists after overstretching without detectably affecting elasticity.

High HMGB concentrations promote formation of an HMGB filament that prevents overstretching

Some DNA stretching curves display shorter overstretching plateaus, particularly at protein concentrations $>1\,\mu M$. Figure 5F shows the overstretchable fraction of the total DNA length as a function of protein concentration, calculated as the apparent DNA overstretching length per bp, Δx, divided by its maximum value, $B_{ss} - B_{ds}$, ($f = \Delta x/(B_{ss} - B_{ds})$, where $B_{ss} - B_{ds} = 0.22\,nm$/bp). The overall magnitude of this effect is modest in the studied range of protein concentrations (up to $4\,\mu M$), reaching at most 20%.

DISCUSSION

Rapid HMGB–DNA microscopic dissociation versus slow macroscopic dissociation

A principal clarifying contribution of this work is the measurement of rapid DNA dissociation rates [$\sim$0.1 to $\sim 6\,s^{-1}$ (Table 2)] for all four HMGB proteins studied here. These rapid DNA dissociation rates agree with recent bulk measurements (26) but contrast with the slow dissociation rates (10^{-2} to 10^{-4} s^{-1}) observed for the same protein preparations on washing (52). Slow dissociation rates were also recently observed for Nhp6Ap and DNA-bending proteins HU and Fis (32,52). Explanations for slow dissociation kinetics included protein–protein-DNA binding cooperativity or sequence-specific protein–DNA interactions. These explanations are not pertinent for the HMGB proteins studied here. We appeal rather to the existence of two distinct protein–DNA dissociation rates: macroscopic and microscopic. Macroscopic dissociation allows proteins to escape into bulk solution. Microscopic dissociation breaks immediate short-range protein–DNA contacts, but the protein remains 'territorially' bound to DNA through long-range electrostatic interaction. Support for a microscopic dissociation process comes from the observation that slow macroscopic dissociation is accelerated by high salt for HU, Fis and HMGB proteins (32). The existence of this process also explains the observation that such proteins can be removed from DNA within seconds by the addition of excess free DNA (52), or exchanged with other proteins in solution at a rate proportional to the protein concentration (30). Previous bulk experiments suggested that the macroscopic dissociation rate could be dramatically reduced simply by reducing the concentration of free HMGB protein through addition of excess carrier DNA (5). As noted by Marko and coworkers (32), there is a notable contradiction between the measured slow protein–DNA dissociation rate, $k_{off,macro}$ $\sim 10^{-2}$ to 10^{-4} s^{-1}, the apparent K_D of 10–100 nM and the observed fast DNA binding at concentrations $c \sim K_D$. The association time τ_{on} (0.1–10 s) suggests a bimolecular association rate of $k_a = 1/(\tau_{on} \cdot K_D)$ $\sim 10^6$–$10^8\,M^{-1}s^{-1}$. The expected dissociation rate for such binding $k_{off} = k_a \cdot K_D = 1/\tau_{on} \sim 0.1$–$10\,s^{-1}$ is much faster than the observed dissociation rate into solution, discussed above. We now measure HMGB–DNA dissociation rates that are in good agreement with the expectations for a bimolecular reaction. We suggest that these rates reflect the microscopic dissociation rates, due to the loss of HMGB–DNA short-range interactions. Breaking such contacts facilitates changes in DNA strand winding. Thus, our novel single-molecule experimental approach measures the characteristic rate at which force-induced DNA unwinding in the presence of HMGB becomes independent of the unwinding rate, yielding estimates of the microscopic dissociation rate for individual HMGB proteins.

Short range HMGB–DNA contacts play the dominant role in HMGB-induced DNA bending

Our measured $k_{\mathrm{off,micro}}$ values of 0.1–10 s^{-1} for the four HMGB proteins studied here span almost two orders of magnitude, with the two slower rates of 0.88 and 0.15 s^{-1} for HMGB2 (box A) and Nhp6Ap, respectively, and the two faster rates of 3.3 and 6.1 s^{-1} for the chimeric HMGB proteins M1 and M2, respectively. As $k_{\mathrm{off,micro}}$ does not reflect the total strength of protein–DNA binding, but rather pertains to the barrier for breaking only local interactions, it is reasonable that the value of $k_{\mathrm{off,micro}}$ does not correlate with apparent K_D, which decreases with the net positive charge of the NTD (Tables 1 and 2). This result reflects the fact that short-range HMGB–DNA contacts are stronger for the two wild-type proteins than the two chimeric proteins. Local contact strength may depend on protein charge in a complicated manner that depends on positioning particular HMGB amino acids within the DNA structures.

The $k_{\mathrm{off,micro}}$ rates correlate directly with the ability of HMGB proteins to compact DNA, characterized in this study by the smaller HMGB-saturated DNA persistence length, and with the ability of HMGB to extend the DNA contour length by intercalation (Tables 1 and 2). Thus, DNA bending by HMGB proteins is more correlated with the strength of local DNA contacts than with N-terminal positive charge. This finding relates to the work of Privalov and coauthors (66–68), decomposing the energetics of HMGB-induced DNA bending into

contributions from short-range interactions versus long-range electrostatic effects. Here we observe that a sequence non-specific HMGB protein with the smallest positive NTD charge, HMGB (box A), induces the largest DNA bend, consistent with stronger local contacts. This result suggests that short-range non-electrostatic interactions are primarily responsible for the DNA bending observed for the series of four proteins studied here.

The slower dissociation rate of the Nhp6Ap protein compared with HMGB2 (box A) measured in this work is consistent with the superior facilitation of DNA cyclization by Nhp6A *in vitro* and *in vivo* (5). Interestingly, Maher and coworkers observed that the chimeric HMGB proteins M1 and M2 studied in this work were almost as effective in promoting DNA cyclization as Nhp6Ap, and much more effective than HMGB2 (box A). This result does not contradict our current conclusion that the M1 and M2 proteins promote less DNA bending, as the DNA-binding affinities of these chimeric proteins are higher, which under conditions of low protein saturation may dominate the overall protein effect on cyclization.

HMGB proteins bind two DNA strands of any secondary structure and winding with fast microscopic kinetics

Measurement of rapid HMGB–DNA microscopic association and dissociation rates depends on recognition of the existence of two kinetic regimes in force-extension experiments. When the complete DNA overstretching and release cycle is performed on a timescale longer than 100 s, the resulting HMGB–DNA force-extension curves appear different than for bare DNA, while displaying reproducibility between cycles and lacking significant hysteresis (Figure 2C and D). As increasing force changes the DNA conformation and the HMGB–DNA binding mode, the effective elastic behavior of the complex, nonetheless, remains well equilibrated, suggesting that the HMGB–DNA association–dissociation kinetics are faster than the DNA stretching process. This situation changes as the time of HMGB–DNA complex stretching becomes <10 s. Before the overstretching transition, changes in the HMGB–DNA force-extension curve with pulling rate are moderate and appear as an increase in persistence length at the highest pulling rates (Figure 5D). There are many possible reasons for this effect, including change in the HMGB–DNA stretching behavior due to the protein-imposed torsional constraint. This constraint becomes more evident as a saturated HMGB–DNA complex is pulled through the overstretching transition at a high rate. The presence of the DNA-bound HMGB protein is only apparent through the effective restriction on DNA unwinding on stretching and DNA re-winding on release. The overstretching plateaus for both torsionally constrained B-form DNA and completely unwound, overstretched and torsionally constrained protein-bound DNA agree with their protein-free values at ~115 and ~50 pN (62). Furthermore, the length and elasticity of the overstretched DNA remain largely unaffected by protein (Figure 5E and F).

These observations imply that all four studied HMGB proteins remain bound to DNA throughout overstretching, strongly interfering with any changes in the linking number of the two DNA strands on short timescale of 0.1–10 s. This result reflects HMGB protein promiscuity in binding to DNA strands with different secondary structures. Although this result was unexpected, it is consistent with the known ability of HMGB proteins to bind many deformed DNA structures, often with greater affinity than to B-form DNA. Indeed, HMGB proteins are known to bind tightly to bent DNA (15), cross-linked DNA (33,69), extruded cruciform DNA (19), locally mismatched and unpaired DNA (70) and supercoiled DNA (71). HMGB proteins thus endow DNA with a flexible hinge-bending mode (27,28) and local softening of DNA torsional rigidity, as was previously observed for the HU protein (32). According to the present work, HMGB proteins transiently introduce such highly deformable sites with microscopic dissociation rates of 0.1–10 s^{-1}.

Functional implications of the ability of HMGB proteins to strongly and transiently deform DNA

The observed rapid microscopic rates of HMGB-induced DNA conformational interconversion facilitate cyclization of short (100–300 bp) DNA fragments and synapsis of DNA sites for transcription factor binding (72). Indeed, HMGB proteins strongly enhance these processes even at low protein concentrations ($c << K_D$), reflecting *in vivo* stoichiometries of one HMGB protein present per several hundreds of genomic DNA base pairs (5). Under such low HMGB-binding conditions, a DNA fragment of the length comparable with its unperturbed persistence length of 50 nm (150 bp) may be bound, on average, by just a few proteins. Such short DNA fragments with few HMGB-induced bends display greatly reduced persistence lengths (72,73). This behavior suggests that the few HMGB-induced DNA bends are not static, but fluctuating on the short timescale of 0.1–10 s, leading to an effective time-averaging rather than length-averaging of the observed DNA–protein complex persistence length.

The ability of HMGB proteins to strongly but transiently bind a wide variety of dsDNA structures may facilitate destabilization of nucleosomes as required for transcription (6,72). Indeed, DNA wound onto nucleosomes is strongly deformed (74,75). The promiscuous HMGB-binding properties discussed above may introduce sites of strong DNA deformability. Based on the results of this study, such deformable DNA sites will not be static, but transient on the timescale of 0.1–10 s. This behavior will soften both structured and unstructured DNA.

The newly discovered ability of the HMGB proteins to constrain DNA winding on short timescales suggests novel physiological functions such as helicase retardation. The present study suggests that an HMGB-bound turn of B-form DNA can unwind on a timescale not faster than several seconds. In the limiting case of HMGB–DNA saturation, the rate of helicase-driven duplex unwinding might then be decreased to 1–10 bp/s. HMGB-type protein binding might slow helicase-driven duplex

unwinding 10- to 100-fold relative to the unwinding rate of free DNA.

SUMMARY

In this work, we stretch single DNA molecules in the presence of four different HMGB proteins to characterize HMGB–DNA interactions. In contrast to previous micromechanical studies of other DNA-bending proteins, we stretch DNA completely through its overstretching transition and follow HMGB effects on both B-form and overstretched DNA. Importantly, we perform a systematic study of the effect of pulling rate on HMGB–DNA stretching curves, allowing characterization of both equilibrium and kinetic parameters for HMGB–DNA interactions. Slow DNA stretch–release cycles (~100 s) appear to be in equilibrium, suggesting that HMGB–DNA on–off processes are fast compared with this timescale for both B-form and overstretched DNA. In contrast, faster stretch–release cycles reveal that the overstretching rate becomes limited by HMGB protein dissociation, allowing calculation of the microscopic dissociation rate. Together with our earlier work, these results suggest that HMGB-induced DNA bends do not have rigid structures, as HMGB proteins are not dissociated by high force. Instead, HMGB binding causes site-specific 'softening' of the DNA duplex, and the average bending angle characterizes more the degree of protein-induced DNA deformation than a particular HMGB-bound DNA conformation. Binding events are sequence non-specific and transient, with rapid kinetics (microscopic residence times ~0.1–10 s) relative to DNA looping and other processes where DNA rigidity is relevant. HMGB-induced DNA bending is unrelated to HMGB–DNA binding cooperativity, which is low. Finally, HMGB proteins bind both DNA strands in many conformations (including overstretched DNA) and inhibit changes in twist on the short timescale of protein dissociation. These important features of HMGB architectural protein function are uniquely revealed through the single-molecule optical tweezers approaches described here.

SUPPLEMENTARY DATA

Supplementary Data are available at NAR Online: Supplementary Tables 1–6, Supplementary Figures 1–6, and Supplementary References [23,39].

ACKNOWLEDGEMENTS

The aurthors are especially grateful for many insightful discussions with Alain Karma.

FUNDING

National Institutes of Health [2R01GM72462 to M.C.W., 2R01GM075965 to L.J.M.]; Mayo Foundation. Funding for open access charge: NIH [GM075965].

Conflict of interest statement. None declared.

REFERENCES

1. Stros,M. (2010) HMGB proteins: interactions with DNA and chromatin. *Biochim. Biophys. Acta Gene Reg. Mech.*, **1799**, 101–113.
2. Bianchi,M.E. (2009) HMGB1 loves company. *J. Leukocyte Biol.*, **86**, 573–576.
3. Lange,S.S., Mitchell,D.L. and Vasquez,K.M. (2008) High mobility group protein B1 enhances DNA repair and chromatin modification after DNA damage. *Proc. Natl Acad. Sci. USA*, **105**, 10320–10325.
4. Liu,Y., Prasad,R. and Wilson,S.H. (2010) HMGB1: roles in base excision repair and related function. *Biochim. Biophys. Acta Gene Reg. Mech.*, **1799**, 119–130.
5. Sebastian,N.T., Bystry,E.M., Becker,N.A. and Maher,L.J. III (2009) Enhancement of DNA flexibility *in vitro* and *in vivo* by HMGB box A proteins carrying box B residues. *Biochemistry*, **48**, 2125–2134.
6. Travers,A.A. (2003) Priming the nucleosome: a role for HMGB proteins? *EMBO Rep.*, **4**, 131–136.
7. Ragab,A. and Travers,A. (2003) HMG-D and histone H1 alter the local accessibility of nucleosomal DNA. *Nucleic Acids Res.*, **31**, 7083–7089.
8. Gerlitz,G., Hock,R., Ueda,T. and Bustin,M. (2009) The dynamics of HMG protein-chromatin interactions in living cells. *Biochem. Cell Biol.*, **87**, 127–137.
9. Bianchi,M.E. and Agresti,A. (2005) HMG proteins: dynamic players in gene regulation and differentiation. *Curr. Opin. Genet. Dev.*, **15**, 496–506.
10. Thomas,J.O. and Travers,A.A. (2001) HMG1 and 2, and related 'architectural' DNA-binding proteins. *Trends Biochem. Sci.*, **26**, 167–174.
11. Travers,A. (2000) Recognition of distorted DNA structures by HMG domains. *Curr. Opin. Struct. Biol.*, **10**, 102–109.
12. Travers,A.A., Ner,S.S. and Churchill,M.E. (1994) DNA chaperones: a solution to a persistence problem? *Cell*, **77**, 167–169.
13. Stott,K., Tang,G.S.F., Lee,K.-B. and Thomas,J.O. (2006) Structure of a complex of tandem HMG boxes and DNA. *J. Mol. Biol.*, **360**, 90–104.
14. Masse,J.E., Wong,B., Yen,Y.-M., Allain,F.H.T., Johnson,R.C. and Feigon,J. (2002) The S. cerevisiae architectural HMGB protein NHP6A complexed with DNA: DNA and protein conformational changes upon binding. *J. Mol. Biol.*, **323**, 263–284.
15. Ohndorf,U.-M., Rould,M.A., He,Q., Pabo,C.O. and Lippard,S.J. (1999) Basis for recognition of cisplatin-modified DNA by high-mobility-group proteins. *Nature*, **399**, 708–712.
16. Allain,F.H.T., Yen,Y.-M., Masse,J.E., Schultze,P., Dieckmann,T., Johnson,R.C. and Feigon,J. (1999) Solution structure of the HMG protein NHP6A and its interaction with DNA reveals the structural determinants for non-sequence-specific binding. *EMBO J.*, **18**, 2563–2579.
17. Murphy,F.V. IV, Sweet,R.M. and Churchill,M.E.A. (1999) The structure of a chromosomal high mobility group protein–DNA complex reveals sequence-neutral mechanisms important for non-sequence-specific DNA recognition. *EMBO J.*, **18**, 6610–6618.
18. Wozniak,K. and Blasiak,J. (2002) Recognition and repair of DNA-cisplatin adducts. *Acta Biochim. Pol.*, **49**, 583–596.
19. Bianchi,M., Beltrame,M. and Paonessa,G. (1989) Specific recognition of cruciform DNA by nuclear protein HMG1. *Science*, **243**, 1056–1059.
20. Dragan,A.I., Klass,J., Read,C., Churchill,M.E.A., Crane-Robinson,C. and Privalov,P.L. (2003) DNA binding of a non-sequence-specific HMG-D protein is entropy driven with a substantial non-electrostatic contribution. *J. Mol. Biol.*, **331**, 795–813.
21. Dragan,A.I., Read,C.M., Makeyeva,E.N., Milgotina,E.I., Churchill,M.E.A., Crane-Robinson,C. and Privalov,P.L. (2004) DNA binding and bending by HMG boxes: energetic determinants of specificity. *J. Mol. Biol.*, **343**, 371–393.

22. Churchill,M.E.A., Klass,J. and Zoetewey,D.L. (2010) Structural analysis of HMGD-DNA complexes reveals influence of intercalation on sequence selectivity and DNA bending. *J. Mol. Biol.*, **403**, 88–102.
23. McCauley,M.J., Zimmerman,J., Maher,L.J. III and Williams,M.C. (2007) HMGB binding to DNA: single and double box motifs. *J. Mol. Biol.*, **374**, 993–1004.
24. Lorenz,M., Hillisch,A., Payet,D., Buttinelli,M., Travers,A. and Diekmann,S. (1999) DNA bending induced by high mobility group proteins studied by fluorescence resonance energy transfer. *Biochemistry*, **38**, 12150–12158.
25. Love,J.J., Li,X., Case,D.A., Giese,K., Crosschedl,R. and Wright,P.E. (1995) Structural basis for DNA bending by the architectural transcription factor LEF-1. *Nature*, **376**, 791–795.
26. Zimmerman,J. and Maher,L.J. III (2008) Transient HMGB protein interactions with B-DNA duplexes and complexes. *Biochem. Biophys. Res. Commun.*, **371**, 79–84.
27. Zhang,J., McCauley,M.J., Maher,L.J. III, Williams,M.C. and Israeloff,N.E. (2009) Mechanism of DNA flexibility enhancement by HMGB proteins. *Nucleic Acids Res.*, **37**, 1107–1114.
28. Zhang,J., McCauley,M.J., Maher,L.J. III, Williams,M.C. and Israeloff,N.E. (2012) Basic N-terminus of yeast Nhp6A regulates the mechanism of its DNA flexibility enhancement. *J. Mol. Biol.*, **416**, 10–20.
29. McCauley,M., Hardwidge,P.R., Maher,L.J. III and Williams,M.C. (2005) Dual binding modes for an HMG domain from human HMGB2 on DNA. *Biophys. J.*, **89**, 353–364.
30. Graham,J.S., Johnson,R.C. and Marko,J.F. (2011) Concentration-dependent exchange accelerates turnover of proteins bound to double-stranded DNA. *Nucleic Acids Res.*, **39**, 2249–2259.
31. van Noort,J., Verbrugge,S., Goosen,N., Dekker,C. and Dame,R.T. (2004) Dual architectural roles of HU: formation of flexible hinges and rigid filaments. *Proc. Natl Acad. Sci. USA*, **101**, 6969–6974.
32. Xiao,B., Johnson,R.C. and Marko,J.F. (2010) Modulation of HU-DNA interactions by salt concentration and applied force. *Nucleic Acids Res.*, **38**, 6176–6185.
33. Klass,J., Murphy,F.I., Fouts,S., Serenil,M., Changela,A., Siple,J. and Churchill,M.E. (2003) The role of intercalating residues in chromosomal high-mobility-group protein DNA binding, bending and specificity. *Nucleic Acids Res.*, **31**, 2852–2864.
34. Chaurasiya,K.R., Paramanathan,T., McCauley,M.J. and Williams,M.C. (2010) Biophysical characterization of DNA binding from single molecule force measurements. *Phys. of Life Rev.*, **7**, 299–341.
35. McCauley,M.J. and Williams,M.C. (2009) Review: optical tweezers experiments resolve distinct modes of DNA-protein binding. *Biopolymers*, **91**, 265–282.
36. Peters,J.P., Becker,N.A., Rueter,E.M., Bajzer,Z., Kahn,J.D., Maher,L.J. III, Michael,L., Johnson,J.M.H. and Gary,K.A. (2011) Quantitative methods for measuring DNA flexibility *in vitro* and *in vivo*. *Methods Enzymol.*, **488**, 287–335.
37. Wenner,J.R., Williams,M.C., Rouzina,I. and Bloomfield,V.A. (2002) Salt dependence of the elasticity and overstretching transition of single DNA molecules. *Biophys. J.*, **82**, 3160–3169.
38. Smith,S.B., Cui,Y.J. and Bustamante,C. (1996) Overstretching B-DNA: the elastic response of individual double-stranded and single-stranded DNA molecules. *Science*, **271**, 795–799.
39. Marko,J.F. and Siggia,E.D. (1995) Stretching DNA. *Macromolecules*, **28**, 8759–8770.
40. Bevington,P.R. and Robinson,D.K. (1992) *Data Reduction and Error Analysis for the Physical Sciences*. McGraw-Hill, New York, NY.
41. Press,W.H., Teukolsky,S.A., Vetterling,W.T. and Flannery,B.P. (2002) *Numerical Recipies in C: The Art of Scientific Computing*. Cambridge University Press, Cambridge.
42. Xiao,B., Zhang,H., Johnson,R.C. and Marko,J.F. (2011) Force-driven unbinding of proteins HU and Fis from DNA quantified using a thermodynamic Maxwell relation. *Nucleic Acids Res.*, **39**, 5568–5577.
43. Vladescu,I.D., McCauley,M.J., Nunez,M.E., Rouzina,I. and Williams,M.C. (2007) Quantifying force-dependent and zero-force DNA intercalation by single-molecule stretching. *Nat. Methods*, **4**, 517–522.
44. Rouzina,I. and Bloomfield,V.A. (1998) DNA bending by small, mobile multivalent cations. *Biophys. J.*, **74**, 3152–3164.
45. Schellman,J.A. (1974) Flexibility of DNA. *Biopolymers*, **13**, 217–226.
46. Kowalczykowski,S., Paul,L., Lonberg,N., Newport,J., McSwiggen,J. and von Hippel,P. (1986) Cooperative and noncooperative binding of protein ligands to nucleic acid lattices: experimental approaches to the determination of thermodynamic parameters. *Biochemistry*, **25**, 1226–1240.
47. McGhee,J.D. and von Hippel,P.H. (1974) Theoretical aspects of DNA-protein interactions: cooperative and non-cooperative binding of large ligands to a one-dimensional homogeneous lattice. *J. Mol. Biol.*, **86**, 469–489.
48. Churchill,M.E., Changela,A., Dow,L.K. and Krieg,A.J. (1999) Interactions of high mobility group box proteins with DNA and chromatin. *Methods Enzymol.*, **304**, 99–103.
49. Slama-Schwok,A., Zakrzewska,K., Leger,G., Leroux,Y., Takahashi,M., Kas,E. and Debey,P. (2000) Structural changes induced by binding of the high-mobility group I protein to a mouse satellite DNA sequence. *Biophys. J.*, **78**, 2543–2559.
50. Cantor,C.R. and Schimmel,P.R. (1998) *Biophysical Chemistry*, 10th edn. W.H. Freeman, New York, NY.
51. Livadaru,L., Netz,R.R. and Kreuzer,H.J. (2003) Stretching response of discrete semiflexible polymers. *Macromolecules*, **36**, 3732–3744.
52. Skoko,D., Wong,B., Johnson,R.C. and Marko,J.F. (2004) Micromechanical analysis of the binding of DNA-bending proteins HMGB1, NHP6A, and HU reveals their ability to form highly stable DNA-protein complexes. *Biochemistry*, **43**, 13867–13874.
53. Shokri,L., McCauley,M.J., Rouzina,I. and Williams,M.C. (2008) DNA overstretching in the presence of glyoxal: structural evidence of force-induced DNA melting. *Biophys. J.*, **95**, 1248–1255.
54. Zhang,X., Chen,H., Fu,H., Doyle,P.S. and Yan,J. (2012) Two distinct overstretched DNA structures revealed by single-molecule thermodynamics measurements. *Proc. Natl Acad. Sci. USA*, **109**, 8103–8108.
55. van Mameren,J., Gross,P., Farge,G., Hooijman,P., Modesti,M., Falkenberg,M., Wuite,G.J.L. and Peterman,E.J.G. (2009) Unraveling the structure of DNA during overstretching by using multicolor, single-molecule fluorescence imaging. *Proc. Natl Acad. Sci. USA*, **106**, 18231–18236.
56. Bosaeus,N., El-Sagheer,A.H., Brown,T., Smith,S.B., Åkerman,B., Bustamante,C. and Nordén,B. (2012) Tension induces a base-paired overstretched DNA conformation. *Proc. Natl Acad. Sci. USA*, **109**, 15179–15184.
57. Fu,H., Chen,H., Zhang,X., Qu,Y., Marko,J.F. and Yan,J. (2011) Transition dynamics and selection of the distinct S-DNA and strand unpeeling modes of double helix overstretching. *Nucleic Acids Res.*, **39**, 3473–3481.
58. Paik,D.H. and Perkins,T.T. (2011) Overstretching DNA at 65 pN does not require peeling from free ends or nicks. *J. Am. Chem. Soc.*, **133**, 3219–3221.
59. Rouzina,I. and Bloomfield,V.A. (2001) Force-induced melting of the DNA double helix: part 1. *Thermodynamic analysis*. *Biophys. J.*, **80**, 882–893.
60. Rouzina,I. and Bloomfield,V.A. (2001) Force-induced melting of the DNA double helix: part 2. *Effect of solution conditions*. *Biophys. J.*, **80**, 894–900.
61. Bianco,P., Bongini,L., Melli,L., Dolfi,M. and Lombardi,V. (2011) PicoNewton-millisecond force steps reveal the transition kinetics and mechanism of the double-stranded DNA elongation. *Biophys. J.*, **101**, 866–874.
62. Leger,J.F., Romano,G., Sarkar,A., Robert,J., Bourdieu,L., Chatenay,D. and Marko,J.F. (1999) Structural transitions of a twisted and stretched DNA molecule. *Phys. Rev. Lett.*, **83**, 1066–1069.
63. Crothers,D.M., Hilbers,C.W. and Shulman,R.G. (1973) Nuclear magnetic resonance study of hydrogen-bonded ring protons in Watson-Crick base pairs. *Proc. Natl Acad. Sci. USA*, **70**, 2899–2901.

64. Paramanathan,T., Vladescu,I., McCauley,M.J., Rouzina,I. and Williams,M.C. (2012) Force spectroscopy reveals the DNA structural dynamics that govern the slow binding of Actinomycin D. *Nucleic Acids Res.*, **40**, 4925–4932.
65. Rouzina,I. and Bloomfield,V.A. (1996) Influence of ligand spatial organization on competitive electrostatic binding to DNA. *J. Phys. Chem.*, **100**, 4305–4313.
66. Privalov,P.L., Dragan,A.I. and Crane-Robinson,C. (2011) Interpreting protein/DNA interactions: distinguishing specific from non-specific and electrostatic from non-electrostatic components. *Nucleic Acids Res.*, **39**, 2483–2491.
67. Privalov,P.L., Dragan,A.I. and Crane-Robinson,C. (2009) The cost of DNA bending. *Trends Biochem. Sci.*, **34**, 464–470.
68. Privalov,P.L., Dragan,A.I., Crane-Robinson,C., Breslauer,K.J., Remeta,D.P. and Minetti,C.A. (2007) What drives proteins into the major or minor grooves of DNA? *J. Mol. Biol.*, **365**, 1–9.
69. Dow,L.K., Jones,D.N.M., Wolfe,S.A., Verdine,G.L. and Churchill,M.E.A. (2000) Structural studies of the high mobility group globular domain and basic tail of HMG-D bound to disulfide cross-linked DNA. *Biochemistry*, **39**, 9725–9736.
70. Cerdan,R., Payet,D., Yang,J.-C., Travers,A.A. and Neuhaus,D. (2001) HMG-D complexed to a bulge DNA: an NMR model. *Protein Sci.*, **10**, 504–518.
71. Sheflin,L.G., Fucile,N.W. and Spaulding,S.W. (1993) The specific interactions of HMG 1 and 2 with negatively supercoiled DNA are modulated by their acidic C-terminal domains and involve cysteine residues in their HMG 1/2 boxes. *Biochemistry*, **32**, 3238–3248.
72. Maher,L.J. III (2011) In: Williams,M.C. and Maher,L.J. III (eds), *Biophysics of DNA-Protein Interactions: From Single Molecules to Biosystems*. Springer, New York, NY.
73. Czapla,L., Peters,J.P., Rueter,E.M., Olson,W.K. and Maher,L.J. III (2011) Understanding apparent DNA flexibility enhancement by HU and HMGB architectural proteins. *J. Mol. Biol.*, **409**, 278–289.
74. Luger,K., Mader,A.W., Richmond,R.K., Sargent,D.F. and Richmond,T.J. (1997) Crystal structure of the nucleosome core particle at 2.8 A resolution. *Nature*, **389**, 251–260.
75. Luger,K. and Richmond,T.J. (1998) DNA binding within the nucleosome core. *Curr. Opin. Struct. Biol.*, **8**, 33–40.